Aeroacoustics of Axisymmetric Single- and Dual-Flow Exhaust Nozzles

Philip R. Gliebe*
General Electric Aircraft Engine Group, Evendale, Ohio
and
Thomas F. Balsa†
General Electric Research and Development Center, Schenectady, N.Y.

A systematic approach to the prediction of jet noise has been developed for conical, conventional bypass, and inverted-flow bypass nozzles. The prediction involves computation of the mean velocity, temperature, and relevant turbulence properties throughout the jet. Each turbulent eddy volume in the jet is treated as a statistically independent radiator of sound embedded in the mean-flowfield. The acoustic/mean-flow interaction is computed from high-frequency asymptotic solutions to Lilley's wave equation. Extensive theory-data comparisons indicate that acoustic/mean-flow interaction plays an important role, and that the prediction method can account for most of the observed characteristics of single- and dual-flow jets.

Nomenclature

A = area
A_i = inner stream area
A_o = outer stream area
AR = area ratio A_o/A_i
c = speed of sound
c_0 = ambient speed of sound
D = nozzle diameter
D_{eq} = equivalent area conical nozzle diameter $=\sqrt{4A/\pi}$
D_i = inner stream nozzle diameter
D_p = primary (high-velocity) stream nozzle equivalent diameter
f = observed 1/3-octave frequency
$H(\mu)$ = source spectrum shape function
H = stagnation enthalpy relative to ambient
H_e = exit plane distribution of H
l = turbulence correlation length scale
OASPL = overall sound pressure level, dB re 0.0002 dyn/cm^2
p = acoustic pressure
R = source-to-observer distance
r = radial coordinate
S = source function
SPL = 1/3-octave sound pressure level, dB re 0.0002 dyn/cm^2
T_T = fluid stagnation temperature
T_0 = ambient temperature
t = time
U = time-mean value of u, x-component of velocity
u = x-component of velocity
u' = fluctuating component of u; also rms value of fluctuating component of u
V = time-mean value of v, r-component of velocity
V_i = jet exit plane velocity in inner stream
V_j = jet exit plane velocity (conical or single-flow nozzle)
V_o = jet exit plane velocity in outer stream
v = radial component of velocity
v' = radial component of turbulent fluctuation velocity
x = axial coordinate
θ = angle between observation vector and x axis
λ = turbulent mixing coefficient
μ = ratio of source frequency to characteristic frequency
ρ = fluid density
ρ_0 = ambient density
ϕ = azimuthal angular coordinate in (y,z) plane
ω = source emission frequency, relative to moving source
ω_0 = source characteristic frequency, relative to moving source

Introduction

In the past few years, considerable progress has been made in quantifying and increasing the understanding of the mechanisms of noise produced by round jets. Extensive and careful measurements[1,2] have provided a substantial data base for investigators. Concurrently, recent advances in theoretical modeling of jet noise characteristics,[3,4] especially the phenomenon of acoustic/mean-flow interaction, have produced rational explanations for many observed characteristics.

A unified aerodynamic/acoustic prediction technique has been developed for assessing the noise characteristics of axisymmetric nozzles. The technique utilizes an extension of Reichardt's method[5] to provide predictions of the jet plume flowfield (velocity, temperature, and turbulence intensity distributions). The fine-scale turbulence, produced in the mixing regions of the jet, is assumed to be the primary source of noise, as in the classical theories.[6] The interaction between the generated noise and the jet plume (sound/flow interaction or fluid shielding) is modeled by an extension of the work of Balsa[7] for high-frequency multipole sources convecting in a parallel shear flow.

These basic modeling elements (flowfield prediction, turbulent mixing noise generation, and sound/flow interaction) have been coupled in a discrete volume-element formulation. The jet plume is divided into elemental volumes, each roughly the size of a representative turbulence correlation volume appropriate to that particular location in

Presented as Paper 77-924 at the AIAA/SAE 13th Propulsion Conference, Orlando, Fla., July 11-13, 1977; submitted Sept. 13, 1977; revision received June 23, 1978.

Index categories: Noise; Aeroacoustics; Jets, Wakes, and Viscid-Inviscid Flow Interactions.

*Senior Engineer, Theoretical Aeroacoustics, Advanced Engineering and Technology Programs Department. Member AIAA.

†Engineer, Applied Mechanics Branch, Power Generation and Propulsion Laboratory.

the plume. Each volume element is assigned its own characteristic frequency, spectrum, and turbulence intensity. The sound/flow interaction effects for each volume element are evaluated from the flow environment at that element. The individual volume elements are assumed to be uncorrelated with each other, so that the total contribution to the farfield is simply the sum of the individual volume element contributions.

Previous methods for predicting jet aeroacoustic characteristics have been confined to round and coannular jets. All of these methods[8-10] either ignore the sound/flow interaction effects completely, or recognize only source convection in the absence of a shrouding flow, which has been shown to give incorrect simulation[1] for all but the lowest jet velocities, especially when predicting sound pressure level spectra at observer angles close to the jet axis.

The following sections describe the evolution of the present aeroacoustic model, which extends the previous work to include mean-flow shrouding effects on a volume-element basis. Results are given which compare the flowfield and acoustic farfield characteristics predicted by this model with measured scale-model data.

Prediction Model Methodology

The development of the present prediction method rests on two primary assumptions: 1) the dominant jet noise mechanism is sound production by the small-scale turbulent structure in the mixing regions of the jet plume; and 2) the propagation of this noise to the farfield observer is significantly altered by the surrounding jet fluid in which the turbulent eddies are embedded and convecting. Assumption 1 is just a restatement of Lighthill's[6] ideas; the additional recognition of sound/flow interaction effects identified by Mani[3,4] is implied by assumption 2.

The model is therefore based on a representation of the jet as a collection of convecting and uncorrelated sources. These sources radiate noise with an intensity spectrum directly related to the local flow properties (i.e., mean velocity, density, and turbulent structure quantities such as intensity, length scale, etc.). The net radiation from each eddy is a function of the flow environment of that eddy and is calculated from the wave propagation through a parallel shear flow model of the jet plume.

The model formulation, described in succeeding sections, follows the sequence of steps listed below:

1) The solution for a unit-strength source embedded in an arbitrary profile shear flow is formulated.

2) The results of step 1 are applied to an ensemble of uncorrelated eddy volumes having specified source strength spectra.

3) Equations are derived relating the local flow properties (mean velocity and temperature profiles, turbulent structure properties) to the source strength spectra.

4) An aerodynamic flowfield model is formulated to provide the required jet mean flow and turbulent structure properties in step 3.

These four steps form the basic building blocks for the unified aeroacoustic jet noise prediction procedure and associated computer program. The next sections briefly describe these building blocks, followed by a description of their integration into a unified aeroacoustic jet noise prediction procedure.

Acoustic Theory

The equation which describes the propagation of sound emitted by the turbulence in a jet was derived by Lilley et al.[11] and is as follows:

$$\frac{1}{c^2} D_*^3 p - D_*(\Delta p) \frac{\mathrm{d}}{\mathrm{d}r}(\log c^2) D_*\left(\frac{\partial p}{\partial r}\right) + 2\frac{\partial U}{\partial r}\frac{\partial^2 p}{\partial x \partial r} = S \quad (1)$$

where

$$D_* = \frac{\partial}{\partial t} + U\frac{\partial}{\partial x} \qquad \text{and} \qquad S = \rho D_*\{\nabla\cdot\nabla\cdot(u'\cdot u')\} \quad (2)$$

In the above, $U=U(r)$, $c=c(r)$, $\rho=\rho(r)$ are the mean jet velocity, speed of sound, and density, respectively. The symbol Δ is the Laplacian operator, t is time, and u' is essentially the turbulent velocity fluctuation. Roughly speaking, S is the noise source strength which drives the acoustic pressure fluctuations p. Equation (1) is a third-order wave equation for the variable p, which explicitly displays the influence of mean velocity $U(r)$ and temperature [through speed of sound $c(r)$] profiles on the propagation of noise. The coordinate system is shown in Fig. 1.

To solve Eq. (1), the profiles $\rho(r)$, $U(r)$, $c(r)$, and the source $S(r)$ must first be prescribed. These are provided by the aerodynamic calculation described in the following section. The Green's function for Eq. (1), when convoluted with the source term S, provides the solution to Lilley's equation. The derivation of the former quantity is given in Refs. 12-14.

From the Green's function, solutions for higher order singularities (dipoles, quadrupoles) can be obtained by differentiating the source solution with respect to source coordinates. The right-hand side of Eq. (1), S, represents a mix of quadrupoles of various orientations. This type of quadrupole mix was examined in detail by Ribner.[15] By employing a model of homogeneous isotropic turbulence in the moving eddy reference frame, and by examining the directional average with respect to the azimuthal coordinate of the sound field, Ribner was able to ascribe "weighting factors" to the various quadrupole contributions. This approach is employed in the present model formulation, utilizing the various quadrupole solutions developed from the high-frequency analysis of Lilley's equation.

The amplitude ascribed to each of these quadrupole types is, crudely speaking of the form

$$\mathrm{d}I(\omega) = \frac{\rho_0 l^3}{c_0^5 R^2}(u')^4\omega^4 H(\mu)\,\mathrm{d}V \quad (3)$$

where $\mathrm{d}I(\omega)$ is the acoustic intensity per elemental jet volume $\mathrm{d}V$, ρ_0 is the ambient density, u' is the local turbulence intensity, $H(\mu)$ is the Fourier transform of the moving-frame space-time cross-correlation of u', and μ is the ratio of emitted frequency ω to characteristic frequency ω_0. Equation (3) is used to calculate the mixing noise amplitude and frequency content for each volume element in the jet.

From the aerodynamic flowfield model (described in the following section), mean velocity, density, and turbulent shear-stress profiles can be computed throughout the jet. This calculation also provides the characteristic strength, frequency, and size of the acoustic convecting quadrupole sources that drive the farfield pressure fluctuations. The characteristic frequency and length scale are determined from the aerodynamic predictions of U and u' utilizing the empirically derived similarity relations of Davies et al.,[16]

$$\omega_0 \sim \partial U/\partial r \qquad l \sim u'/\omega_0 \quad (4)$$

where U is the local mean velocity, u' is the local turbulence intensity, and ω_0 and l are the characteristic frequency and length scale, respectively.

Aerodynamic Flowfield Model

The aerodynamic flowfield is modeled using an extension of Reichardt's[5] theory. This extension consists of superposition of elemental solutions of Reichardt's theory to construct complex flows from nozzles of arbitrary cross-section.[14] Reichardt's theory is based on the experimental

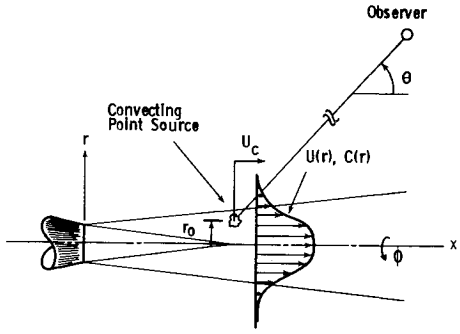

Fig. 1 Jet flow geometry and nomenclature.

observation that the axial momentum profiles in the similarity region of a jet (or wake) are bell-shaped or Gaussian. Utilizing this observation and hypothesizing a proportional relationship between traverse momentum and radial gradient of axial momentum, a linear parabolic governing equation for axial momentum of the diffusion type was deduced. This equation has the following form for axisymmetric flow:

$$\frac{\partial F}{\partial x} = \frac{\lambda}{r}\frac{\partial}{\partial r}\left[\frac{\partial F}{\partial r}\right] \tag{5}$$

where F is the local axial momentum flux $F=\overline{\rho u^2}$, (x,r) are the axial and radial coordinates, respectively, ρ is the local density, and $u=U+u'$ is the local axial velocity. The overbar denotes a time average. The proportionality factor $\lambda=\lambda(x)$ is an empirically determined mixing constant which varies linearly with axial distance along the jet. Similar relations for stagnation enthalpy flux, i.e., $F=\overline{\rho u H}$, where H is the local stagnation enthalpy, can be derived.

In addition to the mean-flow quantities U and ρ, the turbulent shear stress, τ, can be deduced from the Reichardt hypothesis,

$$\tau \approx -\lambda\frac{\partial}{\partial r}(\overline{\rho u^2}) \approx \rho(u')^2 \tag{6}$$

The derivation of the flowfield solution equations is covered in detail in Refs. 14 and 17. The primary assumptions in the above method were: 1) the jet plume mixing occurred at constant static pressure, equal to the ambient value; and 2) the flow was primarily axial with all nozzle exit plane elements in the same plane $x=0$.

Aeroacoustic Model Integration

The basic analytical model elements described in the above sections have been integrated into a unified, aeroacoustic jet noise prediction computational procedure. The jet plume is subdivided into elemental jet volumes, each having its own source strength, spectrum, and flow shrouding. The simple, closed-form solutions permit a rapid, economical computation of the entire jet plume aerodynamic and acoustic characteristics, including farfield spectra at all observer angles. The contributions from each elemental jet volume are simply added on a mean square pressure basis in each frequency band. Input parameters are nozzle exit plane planform geometry and total pressures and temperatures. Aerodynamic output consists of spatial distributions of U, u', and ρ throughout the jet plume. Acoustic output consists of farfield sound pressure level spectra at observer angles 20 deg $\leq\theta_i\geq$ 160 deg, at the arc or sideline distance specified.

Comparison of Predictions with Experiment

The aeroacoustic model described above has been compared with experimental measurements for several jet nozzle types. As mentioned in the Introduction, only axisymmetric nozzles will be examined herein. These include: 1) a conical nozzle, 2) a conventional bypass coplanar coaxial nozzle (i.e., inner velocity higher than outer) and 3) a coplanar, inverted-flow coannular nozzle (inner velocity lower than outer).

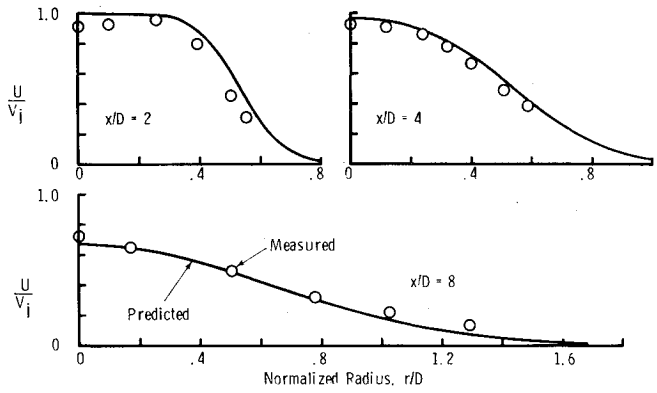

Fig. 2 Comparison of 9.0-cm conical nozzle predicted and measured mean velocity: $V_j=344$ m/s, $T_T=694$ K.

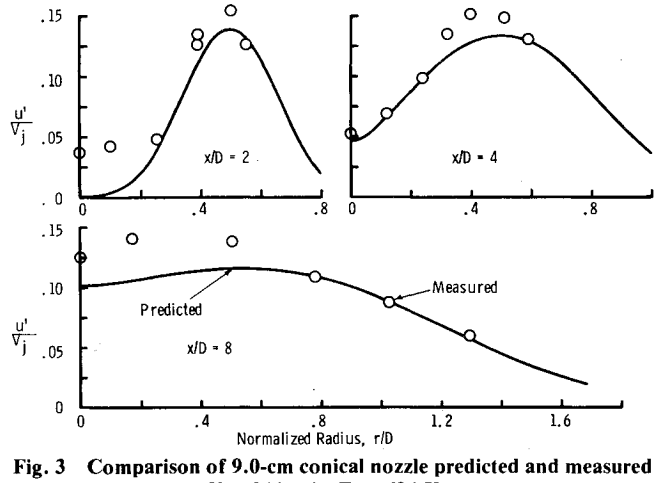

Fig. 3 Comparison of 9.0-cm conical nozzle predicted and measured turbulence intensity: $V_j=344$ m/s, $T_T=694$ K.

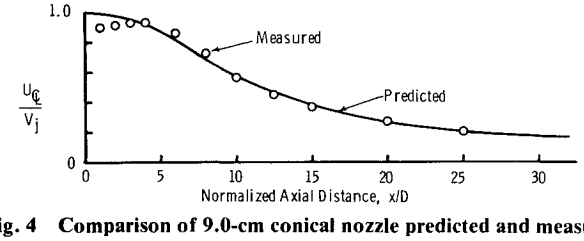

Fig. 4 Comparison of 9.0-cm conical nozzle predicted and measured peak velocity decay: $V_j=344$ m/s, $T_T=694$ K.

Flowfield Comparisons

Flowfield measurements on a high-velocity, high-temperature, scale-model conical jet were made utilizing a laser velocimeter. The measurement system and its characteristics are reported in Ref. 18. Jet plume mean velocity (U) and turbulence velocity (u') measurements were made and compared with theoretical predictions from the above theory in Ref. 17. Figures 2-4 show examples of these comparisons. In general, the agreement between theory and experiment is quite good. The only consistent deviation appears to be near the jet centerline in the transition zone between the potential core (close to the nozzle exit) and the fully developed region far downstream. The theory diffuses the mean momentum too rapidly along the centerline in this transition region, between $4<x/D<10$.

Similar measurements were also made on a scale-model, coplanar, coannular nozzle having a fan-to-primary area ratio

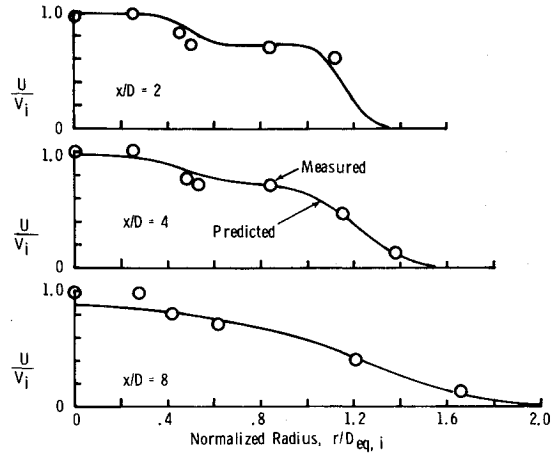

Fig. 5 Conventional bypass AR = 4 coannular nozzle predicted and measured mean velocity: $V_i = 469$ m/s, $V_o = 317$ m/s, $T_{T_i} = 820$ K, $T_{T_o} = 371$ K.

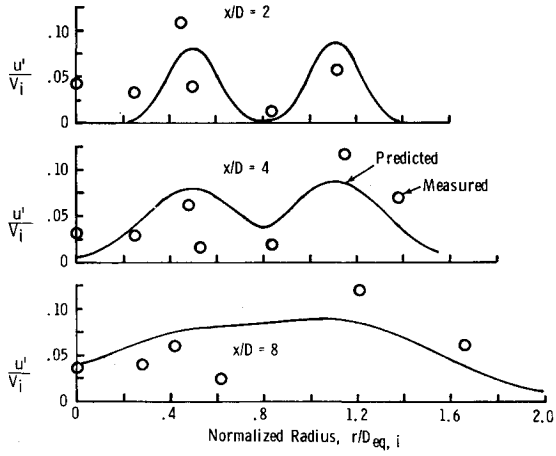

Fig. 6 Conventional bypass AR = 4 coannular nozzle predicted and measured turbulence intensity: conditions as in Fig. 5.

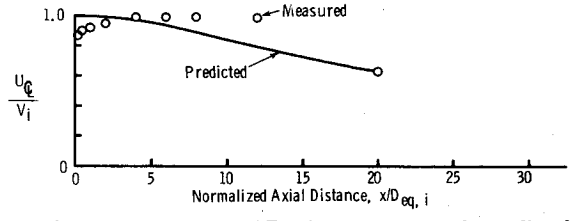

Fig. 7 Conventional bypass AR = 4 coannular nozzle predicted and measured peak velocity decay: conditions as in Fig. 5.

of $A_o/A_i = 4.0$. Comparisons of predicted U and u' distributions with measurements are shown in Figs. 5-7. Again, the agreement is in general satisfactory, although the predicted jet centerline mean velocity decay is more rapid in the transition zone than is indicated by the measurements.

Measurements were made on an inverted-flow scale-model coplanar coannular nozzle having an outer-to-inner ratio of $A_o/A_i = 0.65$. Comparisons of predicted U and u' distributions with measurements are shown in Figs. 8-10. The comparisons are once more quite good, with the same qualification regarding peak velocity decay, which now occurs outboard of the centerline due to the inverted-flow geometry. Two sets of predictions are shown in Figs. 8-10. The solid lines indicate predictions made with the origin $x = 0$ at the nozzle exit plane. However, it can be seen from the data that the flow velocity does not reach its fully expanded value till some distance downstream ($x/D = 1.07$), because the nozzle

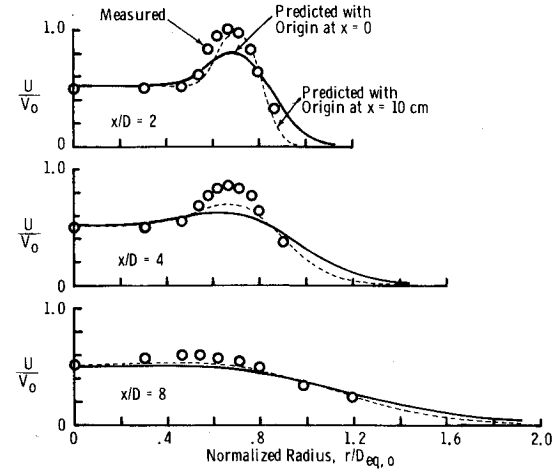

Fig. 8 Inverted-flow AR = 0.65 coannular nozzle predicted and measured mean velocity: $V_i = 366$ m/s, $V_o = 732$ m/s, $T_{T_i} = 552$ K, $T_{T_o} = 891$ K, $D_{eq,0} = 9.48$ cm.

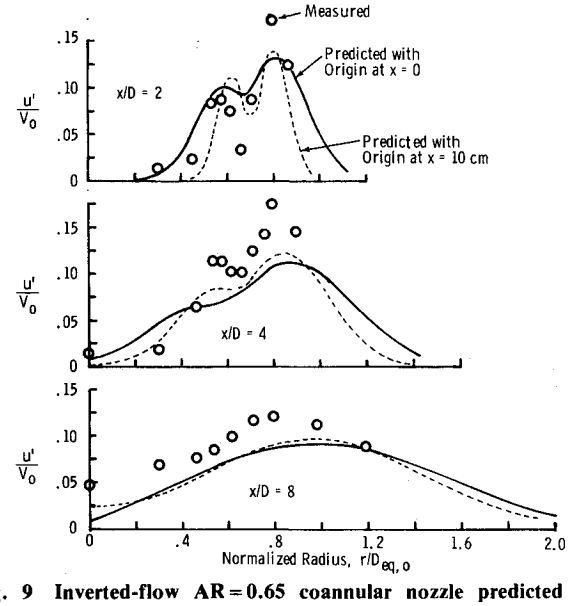

Fig. 9 Inverted-flow AR = 0.65 coannular nozzle predicted and measured turbulence intensity: conditions as in Fig. 8.

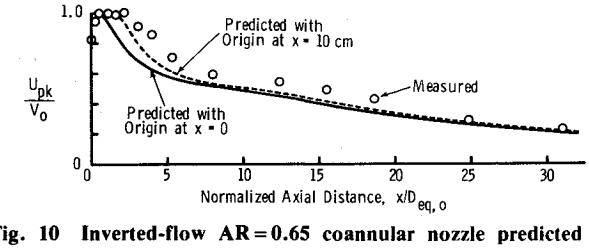

Fig. 10 Inverted-flow AR = 0.65 coannular nozzle predicted and measured peak velocity decay: conditions as in Fig. 8.

pressure ratios are supercritical and additional expansion occurs external to the nozzle. The dashed lines in Figs. 8-10 indicate predictions made with the origin shifted to the location where full expansion has been achieved, $x/D = 1.07$. These predictions agree much better with the measurements, although the differences diminish far downstream.

Farfield Spectrum Comparisons

Many comparisons of the predicted and measured farfield acoustic spectra of conical nozzles have been made using data from several sources. Typical examples of agreement achieved are shown in Fig. 11. These figures display the farfield ob-

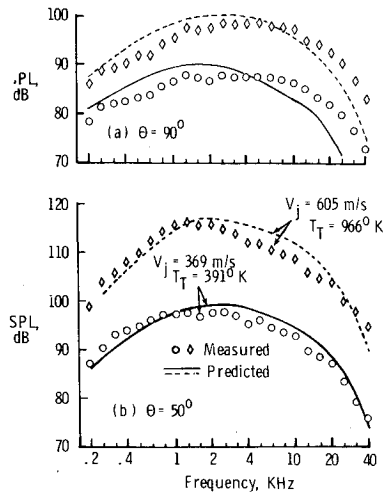

Fig. 11 Conical nozzle predicted and measured SPL spectra.

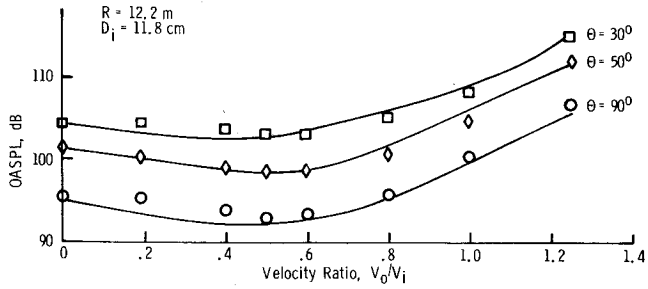

Fig. 12 Comparison of predicted and measured velocity ratio effect on AR = 2.0 conventional bypass jet noise: ——, prediction; □ ◇ ○, measurement.

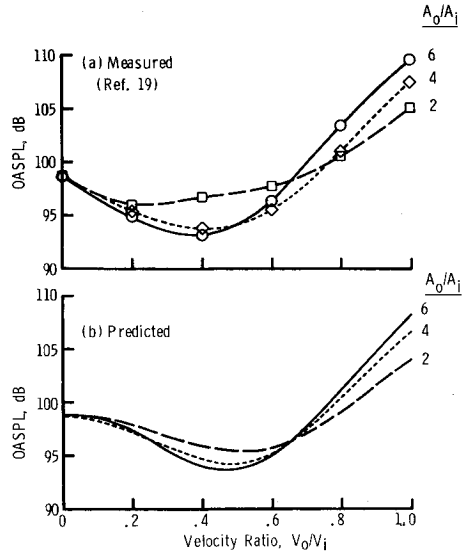

Fig. 13 Influence of AR on conventional bypass jet 90-deg OASPL: $V_i = 305$ m/s, $T_{T_i} = 700$ K, $T_{T_o} = 300$ K.

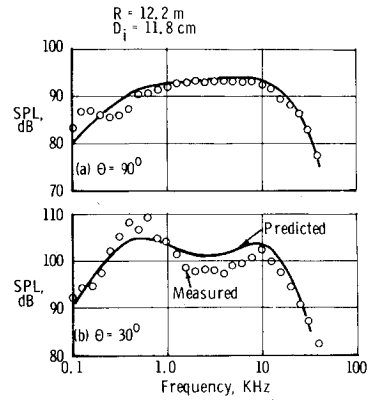

Fig. 14 Comparison of measured and predicted inverted-flow coannular nozzle SPL spectra: $A_o/A_i = 0.4$, $V_o/V_i = 1.5$, $V_i = 366$ m/s, $V_o = 549$ m/s, $T_{T_i} = 556$ K, $T_{T_o} = 667$ K.

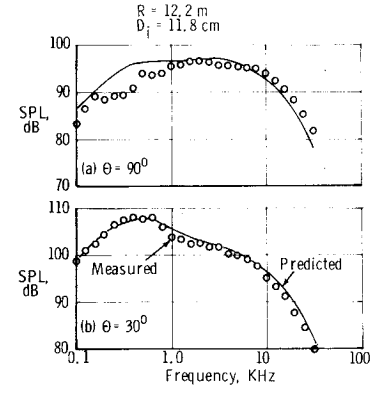

Fig. 15 Comparison of measured and predicted inverted-flow coannular nozzle SPL spectra: $A_o/A_i = 2.0$, $V_o/V_i = 1.5$, $V_i = 305$ m/s, $V_o = 457$ m/s, $T_{T_i} = 294$ K, $T_{T_o} = 556$ K.

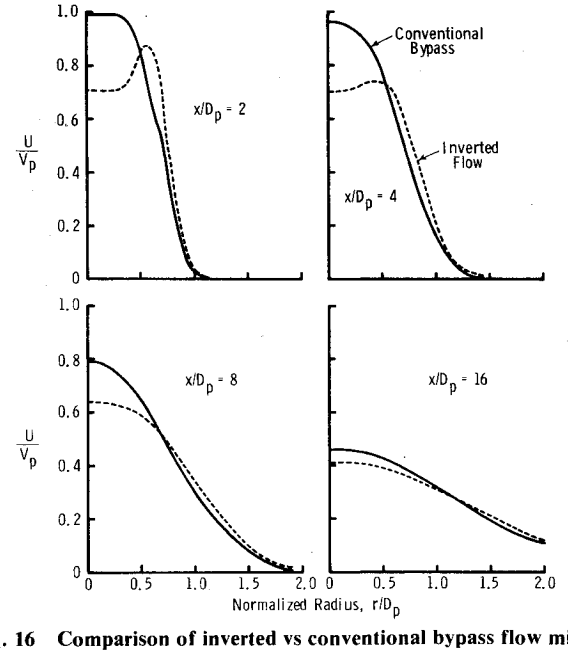

Fig. 16 Comparison of inverted vs conventional bypass flow mixing on mean velocity profiles.

served 1/3-octave sound pressure level spectra at two angles, for a range of jet velocity/temperature combinations. The good agreement indicated by these comparisons demonstrates the ability of the theory to adequately model the variation of noise with jet velocity, temqerature, frequency, and observer angle.

Many data-theory comparisons have been made for conventional bypass coaxial nozzles. The coaxial jet introduces three new variables: 1) area ratio A_o/A_i, 2) velocity ratio V_o/V_i, and 3) temperature ratio T_{T_o}/T_{T_i}. Typical examples of the influence of these parameters on jet noise, both predicted and measured,[19] are shown in Figs. 12 and 13. These example comparisons show satisfactory agreement between prediction and experiment, providing additional verification of the generality of the theoretical model. In particular, the location and magnitude of a noise minimum as velocity ratio is varied is predicted quite well (Fig. 12). This noise minimum is a direct consequence of the reduction in turbulence intensity in the inner-to-outer stream mixing layer as the outer flow velocity is increased to about 40-50% of the inner flow velocity. Further increases in outer flow velocity

cause the outer-to-ambient stream mixing layer turbulence to produce the dominant noise. Another feature of coaxial jets predicted quite well by the theory is the relative insensitivity of noise to area ratio A_o/A_i, for velocity ratios $V_0/V_i < 0.4$.

The recent interest in inverted-flow coannular nozzles for application to low-noise advanced supersonic transport (AST) exhaust systems has prompted an evaluation of the present theoretical model adequacy for predicting the acoustic characteristics of this type of jet. Comparisons were made with scale-model acoustic data for several coplanar coannular inverted-flow jets over a range of velocity levels, velocity ratios, and area ratios. Typical results are shown in Figs. 14 and 15. The ability of the model to predict the key features of inverted-flow coannular jet noise is seen to be quite good. In particular, the relatively flat spectrum shape at $\theta = 90$ deg and the characteristic double-peak spectrum shape at $\theta = 30$ deg are duplicated by the model predictions. The shift in the levels of the high- and low-frequency peaks as area ratio is increased is also well modeled.

Noise Suppression Mechanisms: Conventional Bypass vs Inverted-Flow

Based on the preliminary successes achieved in predicting the aerodynamic and acoustic characteristics of single- and dual-flow nozzles discussed above, it was deemed worthwhile to utilize the theory to analyze the noise suppression mechanisms of coannular nozzles. Of particular interest was how flow inversion (ducting the high-velocity hot stream to the outside) can provide noise benefits for dual-flow exhaust systems.

Theoretical predictions were made of a conventional bypass and an inverted-flow coannular nozzle. The nozzles were sized to give the same thrust, and equal primary (high-velocity) flow areas and secondary (low-velocity) flow areas were maintained. The two nozzles therefore have equivalent thrust, mass flow, primary and secondary stream velocities, and temperatures; the differences in noise should therefore be solely a function of jet plume profile development and mixing. Redefining $VR = V_s/V_p$ and $AR = A_s/A_p$, where subscripts p and s refer to primary (high-velocity) and secondary (low-velocity) streams, respectively, back-to-back calculations of aerodynamic and acoustic characteristics were carried out for $AR = 1.0$ and $VR = 0.7$. Figure 16 shows comparisons of mean velocity profiles at several axial stations. The peak velocity axial decays are shown in Fig. 17. From Figs. 16 and 17 it can be seen that flow inversion produces more rapid plume decay. Figure 18 shows comparisons of axial turbulence velocity, a key ingredient in mixing noise source strength, at several axial stations along the plume. These comparisons show the expected lower turbulence levels at small values of x/D_p for the conventional bypass jet, and correspondingly, the higher levels of turbulence at large x/D_p.

The corresponding farfield acoustic spectrum comparisons are shown in Fig. 19. At $\theta = 90$ deg, the inverted-flow nozzle exhibits higher noise at high frequencies and lower noise at low frequencies. Since the high-frequency noise generally comes from regions close to the nozzle exit, the higher high-frequency noise correlates with the higher turbulence levels at small values of x/D_p, shown in Fig. 18. Similarly, low-frequency noise is primarily from the fully developed regions far downstream, and the lower low-frequency noise of the inverted-flow nozzle correlates with its lower turbulence levels for large x/D_p (Fig. 18).

The results at $\theta = 50$ deg, however, show the inverted-flow jet noise to be lower throughout the spectrum. This is primarily a result of reduced convective amplification, i.e., lower eddy convection speeds. The eddy convection speed is proportional to the peak mean axial velocity, and the comparison of peak velocity curves shown in Fig. 17 implies that the inverted-flow jet exhibits lower convection speeds and therefore reduced convective amplification. Figure 20 shows a comparison of overall sound pressure level (OASPL) vs θ for the two jets. Note the shallower slope of the directivity curve for the inverted-flow jet, a result of reduced convective amplification.

To demonstrate the influence of flow shielding as a sound emission mechanism, the back-to-back calculations were repeated with the shielding effects suppressed. These results are shown in Fig. 21, at $\theta = 30$ deg. Note, first of all, that flow shielding is less for the inverted-flow jet, but that the reduced convective amplification more than compensates for this loss.

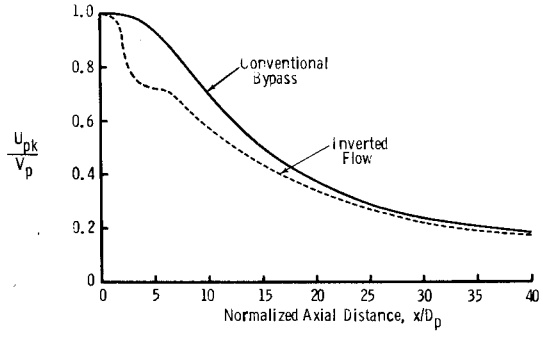

Fig. 17 Comparison of inverted vs conventional bypass flow mixing on peak velocity axial decay.

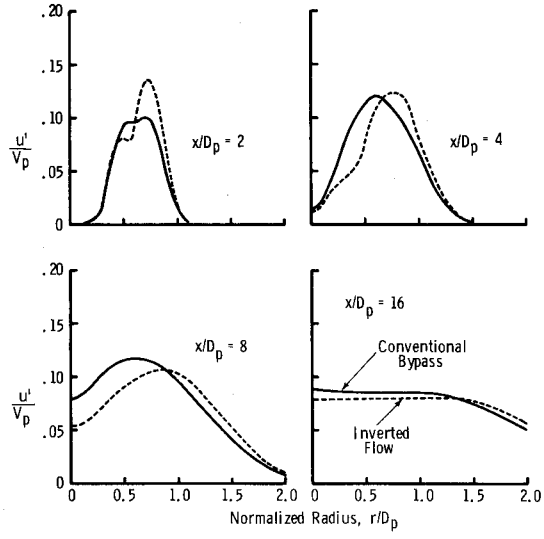

Fig. 18 Comparison of inverted vs conventional bypass flow mixing on turbulence intensity profiles.

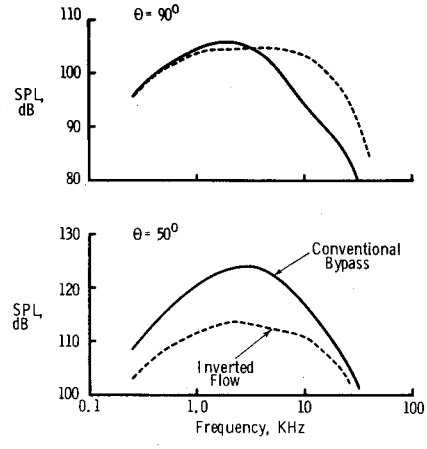

Fig. 19 Comparison of inverted vs conventional bypass flow mixing on SPL spectra.

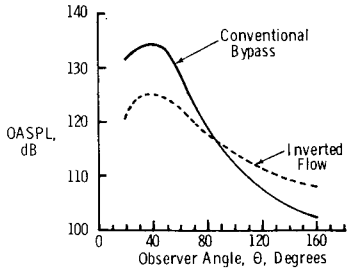

Fig. 20 Comparison of inverted vs conventional bypass flow mixing on OASPL directivity.

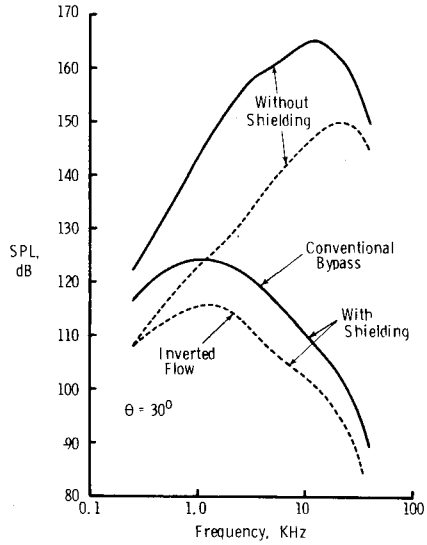

Fig. 21 Influence of flow shielding on inverted and conventional bypass flow jet SPL spectrum.

Concluding Remarks

In summary, comparisons of predictions with experiment have shown that the present theoretical model is capable of predicting many of the observed aerodynamic and acoustic characteristics of single- and dual-flow nozzles. For conventional bypass coaxial jets, the noise reduction was found to be primarily a result of reductions in turbulence intensity. For inverted-flow coannular nozzles, however, the observed noise characteristics were found to be a result of the competing influences of mixing noise, convective amplification, and acoustic shielding alterations. These competing influences are in a delicate balance, and the kind of discrete calculation indicated herein, summing up *all* the contributions to determine the net effect in the farfield, is required to properly predict the noise characteristics of complex nozzles.

Acknowledgments

The authors are grateful to R. Mani of the General Electric Corporate Research and Development Center and E. J. Stringas of the General Electric Aircraft Engine Group for their encouragement, patience, and technical guidance. The work summarized herein was supported by the Federal Aviation Agency under Contract DOT-OS-30034.

References

[1] Lush, P.A., "Measurements of Subsonic Jet Noise and Comparison with Theory," *Journal of Fluid Mechanics,* Vol. 46, Pt. 3, April 1971, pp. 447-500.

[2] Cocking, B.J., "The Effect of Temperature on Subsonic Jet Noise," National Gas Turbine Establishment (U.K.), Rept. R331, May 1974.

[3] Mani, R., "The Jet Density Exponent Issue for the Noise of Heated Subsonic Jets," *Journal of Fluid Mechanics,* Vol. 64, Pt. 3, July 1974, pp. 611-622.

[4] Mani, R., "The Influence of Jet Flow on Jet Noise," *Journal of Fluid Mechanics,* Vol. 73, Pt. 4, Feb. 1976, pp. 753-793.

[5] Reichardt, H., "New Theory of Free Turbulence," *Royal Aeronautical Society Journal,* Vol. 47, 1943, pp. 167-196.

[6] Lighthill, M.J., "On Sound Generated Aerodynamically I. General Theory," *Proceedings of the Royal Society, Series A: Mathematical and Physical Sciences,* Vol. 211, March 1952, pp. 564-587.

[7] Balsa, T.F., "The Far Field of High Frequency Convected Singularities in Sheared Flows, with an Application to Jet Noise Predictions," *Journal of Fluid Mechanics,* Vol. 74, Pt. 2, March 1976, pp. 193-208.

[8] Grose, R.D. and Kendall, R.M., "Theoretical Predictions of the Sound Produced by Jets Having an Arbitrary Cross Section," *ASME Symposium on Fully Separated Flows,* May 1964, pp. 58-63.

[9] Moon, L.H. and Zelazny, S.W., "Jet Noise Modeling: Experimental Study and Models for the Noise and Turbulence Fields," AIAA Paper 74-3, AIAA 12th Aerospace Sciences Meeting, Wash., D.C., Jan. 30-Feb. 1, 1974.

[10] Chen, C.Y., "A Model for Predicting Aero-Acoustic Characteristics of Coaxial Jets," AIAA Paper 76-4, AIAA 14th Aerospace Sciences Meeting, Wash., D.C., Jan. 26-28, 1976.

[11] Lilley, G.M., Morris, P.J., and Tester, B.J., "On the Theory of Jet Noise and its Applications," AIAA Paper 73-987, Aero-acoustics Conference Seattle, Wash., Oct. 15-17, 1973.

[12] Balsa, T.F., "Fluid Shielding of Low Frequency Convected Sources by Arbitrary Jets," *Journal of Fluid Mechanics,* Vol. 70, Pt. 1, July 1975, pp. 17-36.

[13] Balsa, T.F., "The Shielding of a Convected Source by an Annular Jet with an Application to the Performance of Multitube Suppressors," *Journal of Sound and Vibration,* Vol. 44, Jan. 1976, pp. 179-189.

[14] Balsa, T.F., Gliebe, P.R. et al., "High Velocity Jet Noise Source Location and Reduction, Task 2 Final Report: Theoretical Development and Basic Experiments," General Electric Company, CR-FAA-RD-76-79,11, May 1978.

[15] Ribner, H.S., "Quadrupole Correlations Governing the Pattern of Jet Noise," *Journal of Fluid Mechanics,* Vol. 38, Pt. 1, Aug. 1969, pp. 1-24.

[16] Davies, P.O.A.L, Fisher, M.J., and Barratt, M.J., "The Characteristics of the Turbulence in the Mixing Region of a Round Jet," *Journal of Fluid Mechanics,* Vol. 15, March 1963, pp. 337-367.

[17] Gliebe, P.R. and Balsa, T.F., "The Aerodynamics and Acoustics of Coaxial Jets," AIAA Paper 76-492, 3rd AIAA Aeroacoustics Conference, Palo Alto, Calif., July 20-23, 1976.

[18] Knott, P.R. et al., "Supersonic Jet Exhaust Noise Investigation," AFAPL-TR-74-25, June 1974.

[19] Cocking, B.J., "An Experimental Study of Coaxial Jet Noise, National Gas Turbine Establishment (U.K.) Rept. 333, May 1976.